Science Arts & Métiers (SAM)

is an open access repository that collects the work of Arts et Métiers Institute of Technology researchers and makes it freely available over the web where possible.

This is an author-deposited version published in: https://sam.ensam.eu
Handle ID: .http://hdl.handle.net/10985/25923

To cite this version :

Shaolin LIU, Amine BEN ABDELWAHED - Experimental study of capillary impregnation and wettability effects in porous cotton fiber structures - Colloids and Surfaces A p.135995 - 2025

Any correspondence concerning this service should be sent to the repository Administrator : scienceouverte@ensam.eu

Arts et Métiers Institute of Technology

Colloids and Surfaces A: Physicochemical and Engineering Aspects 708 (2025) 135995

Contents lists available at ScienceDirect

Colloids and Surfaces A: Physicochemical and Engineering Aspects

journal homepage: www.elsevier.com/locate/colsurfa

Experimental study of capillary impregnation and wettability effects in porous cotton fiber structures

Shaolin Liu, Amine Ben-Abdelwahed *

Univ. Bordeaux, CNRS, Bordeaux INP, I2M, UMR 5295, F-33400, Talence, France
Arts et Metiers Institute of Technology, CNRS, Bordeaux INP, I2M, UMR 5295, F-33400 Talence, France

GRAPHICAL ABSTRACT

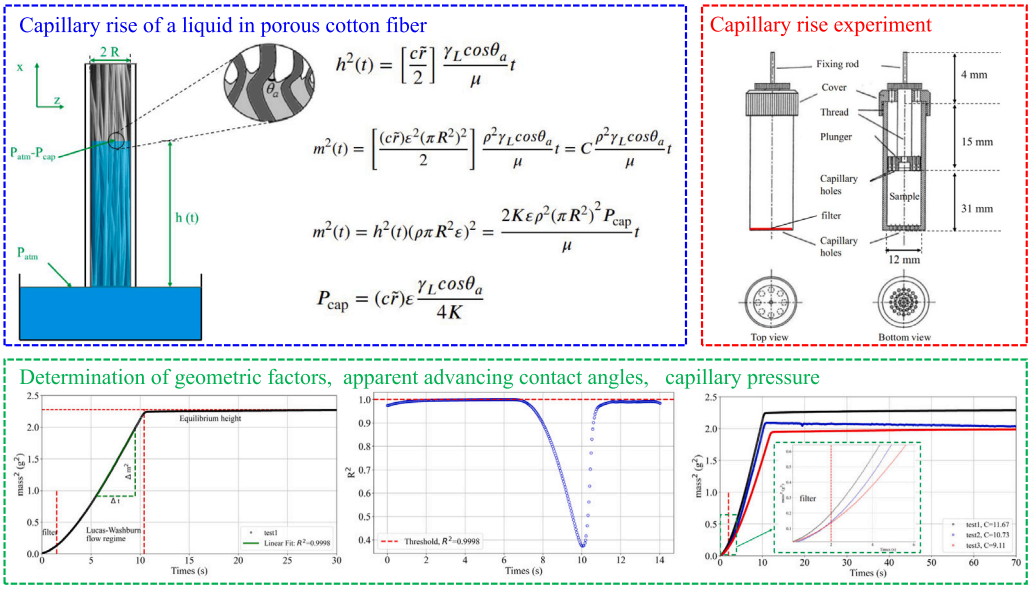

ARTICLE INFO

Keywords:
Porous medium
Impregnation
porosity
Wettability
Capillary constant

ABSTRACT

The study of capillary flows in cellulose fibers is important for various applications, including biomass pyrolysis and drying processes. This work investigates the behavior of cotton fibers during capillary impregnation using a dynamic approach. The analysis utilizes the Washburn equation and tensiometric methods to investigate geometric factors, apparent advancing contact angles, surface free energy of cotton fiber, and capillary pressure. The research is carried out in two phases. The first phase focuses on the theoretical application of the Washburn equation in porous cotton fibers, specifically examining capillary wicking behavior within a cylindrical holder. The second phase involves experimental analysis, using three different liquids: n-heptane, water, and glycerol. The surface tension of the liquids was measured, and the capillary impregnation process was characterized through the determination of geometric factors, apparent advancing contact angles, and surface free energy. The geometrical factors of cotton fibers within the sample holder were found to be 10.39 ± 1.28 mm^5. The apparent advancing contact angles for water and glycerol were $74.93° \pm 2.20°$ and $69.55° \pm 1.83°$, respectively.

* Correspondence to: Arts et Métiers Institute of Technology, 33400, Talence, France.
E-mail address: Amine.BEN-ABDELWAHED@ensam.eu (A. Ben-Abdelwahed).

https://doi.org/10.1016/j.colsurfa.2024.135995
Received 28 October 2024; Received in revised form 28 November 2024; Accepted 15 December 2024
Available online 24 December 2024
0927-7757/© 2024 The Author(s). Published by Elsevier B.V. This is an open access article under the CC BY license (http://creativecommons.org/licenses/by/4.0/).

The surface free energy of cotton fibers was calculated to be 27.82 mN/m. The capillary pressures for n-heptane, water, and glycerol were 2.65 ± 0.33, 2.50 ± 0.31, and 2.91 ± 0.36 kPa for ε=0.483, respectively. The results highlight the relationship between the geometric properties of cotton fibers and the physicochemical characteristics of the liquids during the capillary impregnation process.

Nomenclature

Latin symbols

c	a constant value accounting for the tortuous path of liquid
C	geometric porous medium factor, m^5
F_c	capillary force, N
F_μ	viscous force, N
h	distance traveled by the liquid front, m
K	permeability, m^2
m	mass, kg
p	momentum of the liquid, $kg\,m\,s^{-1}$
P	pressure, Pa
r	radius of the capillary tube, mm
$\tilde{r}$	mean capillary radius of a porous medium, m
R	inner radius of the sample holder, mm
R^2	correlation coefficient
t	time of flow, s
u	equivalent fluid velocity in porous medium, $m\,s^{-1}$
V_f	the original, untreated fiber volume, m^3
V_{final}	the final volume of the sample after compression, m^3
V_{total}	the total volume of the original sample, m^3

Greek symbols

Γ	rate of ascent, $m\,s^{-1}$
γ_L	liquid surface tension, $mN\,m^{-1}$
γ_S	solid surface free energy, $mN\,m^{-1}$
γ_S^+	acid component, $mN\,m^{-1}$
γ_S^-	base component, $mN\,m^{-1}$
γ_S^{AB}	acid–base interactions, $mN\,m^{-1}$
γ_S^{LW}	long-range interactions, $mN\,m^{-1}$
μ	dynamic viscosity of the liquid, $Pa\,s^{-1}$
ρ	density of the liquid, $kg\,m^3$
θ	contact angle, rad
ε	mean porosity

Subscripts

a	advancing
cap	capillary
d	dispersive
p	polar
s	static

1. Introduction

The use of natural fibers (wood fibers, Flax, Cotton, etc.) as biomaterials provides several advantages for eco-materials including eco-friendliness, flexibility, cost reduction, biogenic carbon storage and biodegradation [1,2]. However, natural fibers are hydrophilic materials which are highly sensitive to humidity therefore highly prone to agglomeration. Consequently, a chemical treatment that improves dispersion, adhesion, and compatibility with the matrix fluid (polymeric in general) is recommended [3]. Wet chemical treatment contains several steps (fibers impregnation in an aqueous solution, drying and curing) generating significant effluents, energy consumption and toxic gas emission [4].

Thus, a proper understanding of wetting dynamics is crucial for optimizing these processes, as insufficient impregnation can lead to defects, such as voids or porosities, which negatively impact the quality of the final material [5].

The imbibition of natural fibers is governed by wetting dynamics due to capillary forces [6,7]. These capillary effects are influenced by the physicochemical interactions between fibers and liquids, including the fiber surface energy γ_S and liquid surface tension γ_L, both comprising dispersive γ^d and polar γ^p components, as well as the morphology of the solid substrate or fibrous preform [8,9]. Typically, the contact angle θ between the liquid and the solid surface is measured under static conditions [10]. However, as the flow front advances, a dynamic advancing contact angle (or apparent advancing contact angle) θ_a must be considered [11,12]. Additional assumptions are commonly made, such as the no-slip condition at the dynamic contact line between fluids and solid walls, where friction forces are important (no prewetting lubricant film) [13–15].

In the study of capillary rise dynamics, the roles of inertial forces, viscous forces, and gravity are frequently discussed [16–19]. Understanding which forces dominate at different stages of the process is important. All equations used to predict meniscus height rely on certain assumptions, and these assumptions often involve neglecting specific forces, thereby limiting the reliability of the derived solutions [16]. For modeling porous fibrous media, the substrate is often represented as an array of parallel micro-cylinders [20,21]. Lucas and Washburn [22,23] were among the first to provide an analytical solution describing fluid flow in a capillary tube. However, their law has several limitations: It lacks a gravity term, making it unable to capture the initial stage of meniscus rise. It is based on Poiseuille flow within the capillary tube, where the velocity follows a parabolic profile, which is not applicable near the tube entry.

Numerous studies have explored the different stages of capillary rise dynamics, which are generally divided into four stages: purely inertial stage, visco-inertial stage, purely viscous stage, and viscous-gravitational stage [16,24]. Stange et al. [25] distinguished these stages by using dimensionless numbers, dividing the capillary-driven flow into three regimes: inertial, convective losses, and viscous forces. Zhmud et al. [26] proposed finite and infinite asymptotic solutions for different time scales, while Fries and Dreyer [16] developed an analytical solution for fluid motion in a capillary tube that includes the gravitational term, enabling the prediction of long-term fluid rise behavior. Several studies have approached the problem by numerically solving the full momentum balance equation [24,27]. Ichikawa et al. [28] compared various earlier works, presented experimental results, and conducted a dimensional analysis. Hamraoui et al. [29] used high-speed imaging to study the capillary rise dynamics of ethanol and its mixtures. They demonstrated that inertial effects are significant in the early phase of fluid rise, especially for capillaries with larger radii. Quéré et al. [30] focused on the inertia-dominated flow regime, while other research has examined the influence of dynamic contact angles [10,11]. In the later stages of capillary rise (as $t \to \infty$), the effects of gravity become more prominent, as discussed in the work of Zhmud et al. and Fries et al. [16,26]. Most of these studies concentrate on the transition from inertial to viscous flow in a capillary tube. However, relatively few

studies have addressed the initial acceleration phase of capillary rise dynamics or the behavior of capillary wicking in a porous medium within a cylindrical holder, which remains a less explored area.

The objective of the present work is to examine the influence of the structure of natural fibers and various liquids on their long-term wetting behavior, with experimental research conducted specifically on cotton fibers. Key parameters such as the geometric factors of cotton fibers, the apparent advancing contact angles, the surface free energy of cotton fiber, and the capillary pressure for three liquids with different viscosity were determined. The article is structured as follows: Section 2 introduces the concept of capillary wicking in a porous medium (cotton fiber) within a cylindrical holder, based on the Washburn approach, along with the relevant theoretical equations. The formula for calculating the permeability of compressed cotton fiber samples was also provided. In Section 3, the experimental materials and methods are described, specifically focusing on the use of one solid (cotton fiber) and three liquids (n-heptane, water, glycerol). The objective of the experiments is to investigate the effects of various parameters on capillary pressure during the spontaneous infiltration of natural fibers (cotton fibers). Section 4 discusses the experimental results, where parameters such as the geometric factors, apparent advancing contact angles, and surface free energy of cotton fiber are determined. Additionally, a straightforward method for selecting the linear fitting interval from the experimental data is introduced. Finally, concluding remarks are provided in Section 5.

2. Capillary progression in porous cotton fiber

This section consists of two parts. First, a brief review of the capillary rise of a liquid in a cylindrical tube as described by the Washburn equation is provided. Second, the modified Washburn approach, which applies to the capillary rise of a liquid in a porous medium, specifically porous cotton fibers, is introduced.

2.1. Capillary rise of a liquid in a cylindrical tube

The Washburn equation describes the capillary rise within a cylindrical tube as a result of the competition between viscous forces and surface tension [10,24], as shown in Fig. 1(a). It is more accurate to use the apparent advancing contact angle (θ_a) in the Washburn equation, rather than the static contact angle (θ), especially when gravity effects become important (as described by Jurin's law [6]). The capillary force (F_c) is given by:

$$F_c = 2\pi r\gamma_L cos\theta_a \tag{1}$$

where r refers to the radius of the capillary tube, and γ_L represents the surface tension of the liquid. The viscous force (F_μ), following Poiseuille's law, can be written as:

$$F_\mu = 8\pi\mu h\frac{dh}{dt} \tag{2}$$

where h is the distance traveled by the liquid front, and t is the time of flow. Thus, the Washburn equation represents the balance between these two forces, which, after time integration (starting with the initial condition, $h(t=0)=0$), can be expressed as [8]:

$$h^2(t) = \frac{r}{2}\frac{\gamma_L cos\theta_a}{\mu}t \tag{3}$$

where $h(t)$ represents the depth of liquid intrusion, μ is the liquid dynamic viscosity. The corresponding liquid mass (m) gain over time can then be written as [17]:

$$m^2(t) = \frac{\pi^2 r^5}{2}\frac{\rho^2\gamma_L cos\theta_a}{\mu}t \tag{4}$$

where ρ is the liquid density.

Consequently, the Washburn equation is valid only for the visco-capillary regime, meaning it does not account for the inertial regime (rapid ascent during the initial phase of the flow at very short times) or the gravitational effects (when the fluid meniscus reaches equilibrium). The law loses its physical meaning at very short times when t approaches 0, as the velocity tends to infinity (dh/dt). In reality, the inertial regime must be considered at the onset, which is linked to the fluid's kinetic energy. Quéré et al. [30] suggest that only capillary forces are significant at very short times. The corresponding law by Quéré is expressed as:

$$\frac{dp}{dt} = 2\pi r\gamma_L cos\theta_a; \quad p = m\frac{dh}{dt}; \quad m = \rho h\pi r^2 \tag{5}$$

where p is the momentum of the liquid and m is the mass of the liquid column. This relation can be rewritten as:

$$\left(\frac{dh}{dt}\right)^2 + h\left(\frac{d^2h}{dt^2}\right) = \frac{2\gamma_L cos\theta_a}{\rho r} \tag{6}$$

A detailed numerical solution and analysis of this equation (Eq. (6)) is provided in Appendix. Appendix to demonstrate the rapid initial acceleration of the liquid column driven by capillary forces. For short times (as t approaches 0), the rate of ascent Γ (dh/dt) becomes constant and equals:

$$\Gamma = \left(\frac{2\gamma_L cos\theta_a}{\rho r}\right)^{1/2} \tag{7}$$

2.2. Capillary rise of a liquid in a porous medium

Considering only the contributions of capillary and viscous forces, for an ideal porous medium packed into a column, modeled as a bundle of separated capillary tubes with an average capillary radius, the Washburn law can be expressed as [17]:

$$h^2(t) = \left[\frac{c\tilde{r}}{2}\right]\frac{\gamma_L cos\theta_a}{\mu}t \tag{8}$$

where c is a geometric constant accounting for the tortuous path of the liquid, and it is inversely related to tortuosity. $\tilde{r}$ is the mean capillary radius. For a porous medium packed in a cylindrical container with relative porosity ε, the squared mass can be written as:

$$m^2(t) = \left[\frac{(c\tilde{r})\varepsilon^2(\pi R^2)^2}{2}\right]\frac{\rho^2\gamma_L cos\theta_a}{\mu}t = C\frac{\rho^2\gamma_L cos\theta_a}{\mu}t \tag{9}$$

where R is the inner radius of the sample holder (Fig. 1(b)), and C a geometric porous medium factor. Following the form of Eqs. (5) and (6), the expression for a fiber foam medium within a cylindrical container can be written as follows:

$$\frac{dp}{dt} = 2\pi c\tilde{r}\gamma_L cos\theta_a; \quad p = m\frac{dh}{dt}; \quad m = \rho h\varepsilon\pi R^2 \tag{10}$$

$$\left(\frac{dh}{dt}\right)^2 + h\left(\frac{d^2h}{dt^2}\right) = \frac{2c\tilde{r}\gamma_L cos\theta_a}{\rho\varepsilon R^2} \tag{11}$$

Similarly, for short times (as t approaches 0, $h(t)$ approaches 0, the rate of ascent Γ (dh/dt) in the porous fiber medium becomes constant and can be expressed as:

$$\Gamma = \left(\frac{2c\tilde{r}\gamma_L cos\theta_a}{\rho\varepsilon R^2}\right)^{1/2} \tag{12}$$

Flow through a porous medium is typically modeled using Darcy's law, which relates fluid velocity u to pressure drop dP via permeability K, characterizing the medium's ability to allow liquid with a given viscosity μ to pass through:

$$u = -\frac{K}{\mu}\frac{dP}{dh} \tag{13}$$

The porosity ε of the porous medium can be used to relate the equivalent Darcy velocity u to the distance $h(t)$ traveled by the flow front during filling:

$$\frac{h(t)}{t} = \frac{u}{\varepsilon} = -\frac{K}{\varepsilon\mu}\frac{dP}{dh} = -\frac{K}{\varepsilon\mu}\frac{(P_{atm}-P_{cap})-P_{atm}}{dh} = \frac{K}{\varepsilon\mu}\frac{P_{cap}}{dh} \tag{14}$$

where the capillary pressure (P_{cap}) represents the capillary wicking behavior in an equivalent homogeneous porous medium, as shown in

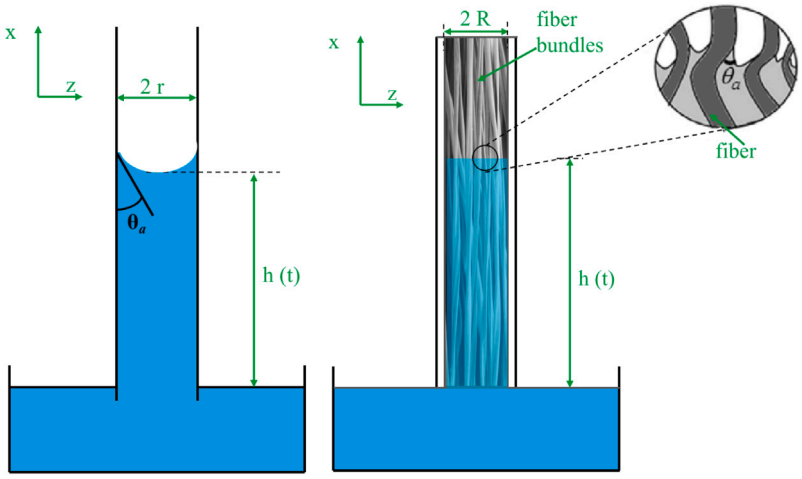

(a) capillary rise in a tube (b) capillary wicking through a bundle of cotton fibers

Fig. 1. Schematic representation of capillary rise.

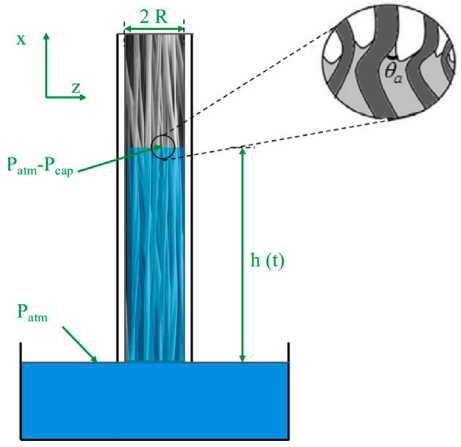

Fig. 2. Capillary wicking in a porous medium based on Darcy's law [17].

Fig. 2. By performing time integration on both sides of the equation, the following relationships for the height $h(t)$ and mass $m(t)$ as functions of time t can be derived, similar to the forms of Eqs. (8) and (9).

$$h^2(t) = \frac{2K P_{\text{cap}}}{\varepsilon \mu} t \tag{15}$$

$$m^2(t) = h^2(t)(\rho \pi R^2 \varepsilon)^2 = \frac{2K\varepsilon\rho^2(\pi R^2)^2 P_{\text{cap}}}{\mu} t \tag{16}$$

By comparing the form of $h^2(t)$ in Eqs. (8) and (15), the capillary pressure P_{cap} can be expressed as follows:

$$P_{\text{cap}} = (c\tilde{r})\varepsilon \frac{\gamma_L cos\theta_a}{4K} \tag{17}$$

where the permeability K specifically refers to the permeability along the cotton fibers, assuming a hexagonal arrangement of the fibers, and is defined as [31,32]:

$$K = \frac{8{r_f}^2}{53} \frac{\varepsilon^3}{(1-\varepsilon)^2} \tag{18}$$

where r_f is the single fiber diameter. For compressed cotton samples, the permeability K is around 6.36×10^{-12} m^2, which will be discussed in detail in Section 4.3.

Table 1
Some physical and mechanical properties of cotton fiber [4].

Density (g/cm^3)	Fiber diameter (μ m)	Tensile strength (Mpa)	Young's modulus (Gpa)	Elongation at break %
1.5	12–25	287–800	5.5–12.6	7.1–8.0

3. Materials and experiments

The tests conducted in this study aim to investigate the effects of various parameters on capillary pressure during the spontaneous infiltration of natural fibers (cotton fibers). Three test liquids: n-heptane, water, and glycerol—were used in the experiments. Fiber samples were placed in a sample holder for wicking tests. First, test curves were obtained using a tensiometric method, and the modified Washburn equation (Eq. (9)) was applied to determine parameters such as the geometric factor C and the apparent dynamic contact angle θ_a.

3.1. Materials

This subsection primarily describes the solid and liquid materials used in the tests, along with their geometric parameters and physical properties.

3.1.1. Cotton fiber

The material used is natural cotton fiber sourced from China. The sample consists of 180 stacked rectangular sheets, with the dimensions of a single sample: length (along fiber orientation), width (perpendicular to the fibers), and height are 60 mm × 50 mm × 7.7 mm, respectively, giving a volume of 2.31×10^4 mm^3 per sample. The mass variation between samples is minimal. For instance, in four random tests, the mass of individual samples was recorded as 0.607 g, 0.608 g, 0.608 g, and 0.608 g, with the maximum deviation not exceeding 0.001 g. The fiber density is around 1.50 g/cm^3, as referenced in the literature [4]. So the original porosity of the uncompressed sample can be calculated as:

$$\varepsilon = 1 - \frac{V_f}{V_{total}} = 1 - \left(\frac{0.608\ \text{g}}{1.5\ \text{g/cm}^3}\right) * \frac{1}{23.1\ \text{cm}^3} = 0.98 \tag{19}$$

where V_f is the fiber volume, V_{total} is the total volume of the original sample. The diameters of individual fibers ranged between 12 and 2 μm. Other parameters, such as tensile strength, Young's modulus, and elongation at break, are provided in Table 1.

Table 2
Some key properties of the test liquids at 20 °C used in the experiments [33].

Liquids	Density ρ (kg/m^3)	Dynamic viscosity μ (kg. m^{-1}. s^{-1})	Surface tension dispersive part $\gamma_L{}^d$ or γ_L^{LW}	polar part $\gamma_L{}^p$ or $\gamma_L{}^{AB}$	acid component γ_L^+	base component γ_L^-	total γ_L (mN/m)
n-heptane	684	0.402×10^{-3}	20.10	0	0	0	20.10
Water	1000	1.002×10^{-3}	21.75	51.00	25.5	25.5	72.75
Glycerol	1261	1.490	37.00	26.00	3.92	57.4	63.00

3.1.2. Test liquids

Three liquids were selected for the study: n-heptane, water, and glycerol. Initially, n-heptane was chosen to determine the geometric factor C of the fibrous medium due to its zero contact angle, making it a perfectly wetting fluid on wettable surfaces. Once the geometric factor was established from this initial step, two additional fluids with distinct properties – water and glycerol – were selected. This method helps reduce the number of unknowns in Eq. (9), allowing for the calculation of advancing contact angles based on the established geometric factor. The properties of these liquids, listed in Table 2, were measured with further details provided in previous studies [33]. Where the surface tension (γ_L), consisting of a dispersive component (γ_L^d or γ_L^{LW}) and a polar component (γ_L^p or γ_L^{AB}), is an important parameter influencing fiber and fluid matrix adhesion [34]. When using the vOCG method [35] to calculate surface free energy, the polar component is further divided into an acid component (electron-acceptor: γ_L^+) and a base component (electron-donor: γ_L^-), as discussed in detail in Section 4.2.3.

3.2. Capillary rise experiment methods

Experimental methods for studying the wettability and impregnation of a solid by a fluid are primarily based on two approaches: visual observation and weighing. In this study, the weighing method was employed using a tensiometer (tensiometric method). This approach has been widely applied in various scientific publications to investigate capillary impregnation in fibrous media, enabling the determination of the capillary constant and dynamic contact angle [8,17].

3.2.1. Tensiometric method

The tensiometric method enables the spontaneous capillary wicking effect and allows for the analysis of wetting behavior. A KRÜSS tensiometer (K100) was used to perform dynamic capillary wicking tests. This tensiometer is equipped with an electronic microbalance (with a resolution of 10 μg) on which the sample holder is secured. During the tests, it was observed that the temperature ranged between 18 °C and 20 °C. For the various capillary wicking tests, the liquid crystallizer moves at a speed of 20 mm/min until the sample holder is detected, meaning the point at which the liquid contacts the sample holder. Due to the varying viscosities of the different liquids, two hold periods were used (120 s and 1800 s). Once contact is made, the recording begins, and the experimental variation of mass over time is obtained.

3.2.2. Experimental protocol

The sample preparation process can be roughly divided into several steps:

1. Begin by tightly rolling the entire sample, ensuring that the direction of the fibers aligns with the orientation of the Washburn cell (as shown in Fig. 3(a)). This step is critical as it allows the fibers to be properly aligned for accurate measurement during the capillary action test.
2. Place a paper filter ((as shown in Fig. 3(b))) at the bottom of the Washburn cell to create a barrier between the rolled sample and the base of the cell. Once the filter is securely in place, carefully insert the tightly rolled sample into the Washburn cell, ensuring that it fits snugly (as shown in Fig. 3(c)) .
3. Apply the maximum weight (as recommended for the Washburn test) to the Washburn cell, pressing down on the probe and the rolled sample five times to ensure sufficient initial compression. This step helps remove any air pockets and ensures uniform contact between the sample and the cell walls.
4. After the initial compression, insert a small metal cylinder into the Washburn cell. This cylinder acts as an additional weight and helps distribute pressure evenly across the sample.
5. Once the cylinder is in place, apply the maximum weight to the Washburn cell another five times (as shown in Fig. 3(c)). This ensures the sample is further compressed and fully prepared for the test, eliminating any inconsistencies in the packing of the fibers.
6. Next, screw the spacer down to its minimum setting. This spacer ensures that the sample remains in place and does not move during the testing process. Ensure that the spacer is tightly fitted and properly adjusted to provide a secure environment for the textile.
7. Finally, tighten the spacer to the Washburn cell, making sure that everything is securely fastened. The final dimensions are displayed in Fig. 3(d).

3.2.3. Sample holder

The sample holder, into which the fibers were introduced, is a hollow cylinder with an inner radius of $R = 6$ mm and a height of $H = 46$ (15+31) mm, as shown in Fig. 3(d). It is equipped with an adjustable piston of $L = 19$ mm, which allows for compression of the samples to achieve a uniform shape. By knowing the geometric parameters of the sample holder, the compression rate can be determined using the fixed 4 mm gap, which provides a percentage measure of how much the sample is compressed. The sample holder is washed with distilled water and dried after each manipulation to remove any contaminants. The porosity (compression rate) of material (ε) is determined by comparing the final volume of the sample after compression, V_{final}, with its initial volume, $V_{initial}$ (which refers to the volume of the sample after being rolled and placed into the Washburn cell, not the original untreated sample volume, as shown in Fig. 3(e)), using the following equation:

$$\varepsilon = 1 - \frac{V_{final}}{V_{initial}} = 1 - \frac{\pi \times 6^2 \times 31}{\pi \times 6^2 \times 60} = 0.483 \tag{20}$$

where 6 mm represents the radius of the sample holder, 31 mm is the height of the sample after compression, and 60 mm refers to the initial height of the sample placed in the sample holder before compression. Note that the porosity obtained here differs from that in Eq. (19), as they represent different concepts.

4. Results and discussion

This section is divided into three main parts. First, the geometric factors of cotton fibers are determined using n-Heptane as the test fluid. In the second step, the apparent advancing contact angles are calculated using water and glycerol as fluids, incorporating the geometric factors obtained in the previous step. Finally, the capillary pressure is calculated based on the values of the geometric factors, apparent advancing contact angles, and permeability.

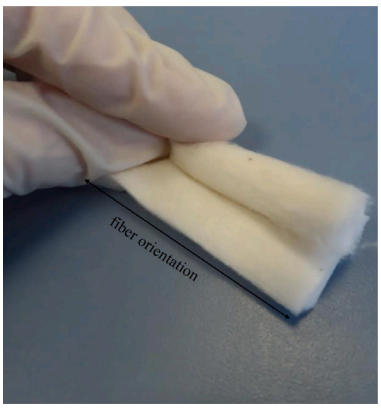

(a) rolling the sample

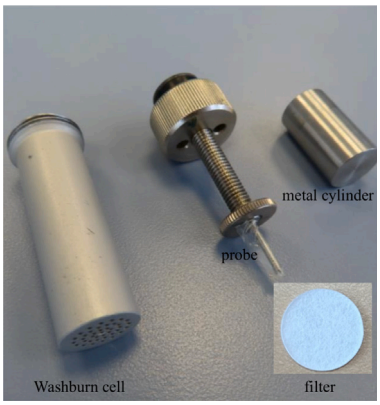

(b) photos of experimental components

(c) put sample inside Washburn cell

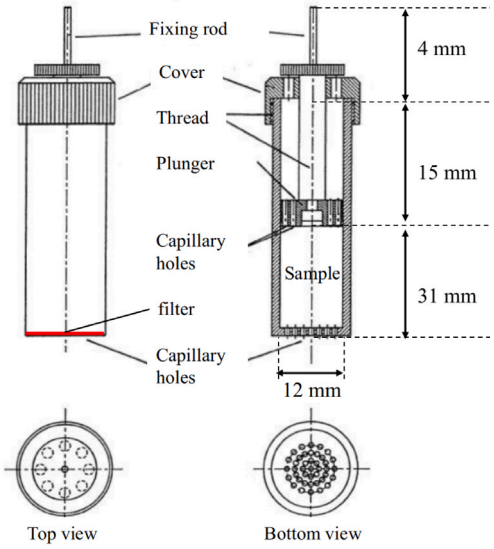

(d) sample holder structure and dimensions (made by KRÜSS GmbH)

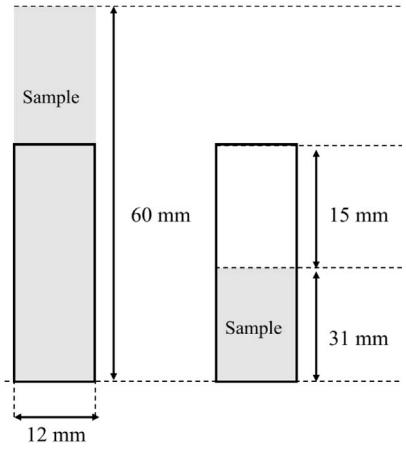

(e) sample volume before and after compression

Fig. 3. Schematic diagram of sample preparation.

4.1. Determination of geometric factors

To characterize capillary impregnation, the first parameter that needs to be determined is the geometric factor (C or $c\tilde{r}$), which is described by the Washburn equation adapted for fibrous media (Eq. (9)). It is important to note that before data acquisition, the mass of the sample holder is tared on the balance to ensure accurate measurements. The curve starts at zero, and three distinct phases can be observed: the first linear region, influenced by the paper filter, followed by a second linear phase (Lucas–Washburn flow), and finally a stable phase (equilibrium height), as shown in Fig. 4.

To determine the value of the geometric factor, the linear region of the m^2 vs t curve must be selected, corresponding to the Lucas–Washburn flow regime. Typically, this linear section is chosen based on experience, as shown in Fig. 4, which introduces an uncertainty in the results. To obtain more accurate results, a Python script was developed. The script performs a sliding intervals linear regression on a dataset, calculating the slope ($\Delta m^2/\Delta t$) and correlation coefficient R^2 for each segment [36]. For instance, the fitting interval length is set to 4 s, and the R^2 threshold to 0.9998. The first interval fits the data from (0, 4), the second from (0.04, 4.04), the third from (0.08, 4.08), and so on. Data for $t \leq 15s$ is processed, since beyond 15s the stable phase is clearly observed, as indicated in Fig. 4. Linear regression is performed for each sliding interval and both the R^2 value and slope ($\Delta m^2/\Delta t$) are recorded. intervals, where R^2 exceeds the threshold, are then identified, and the corresponding results are output.

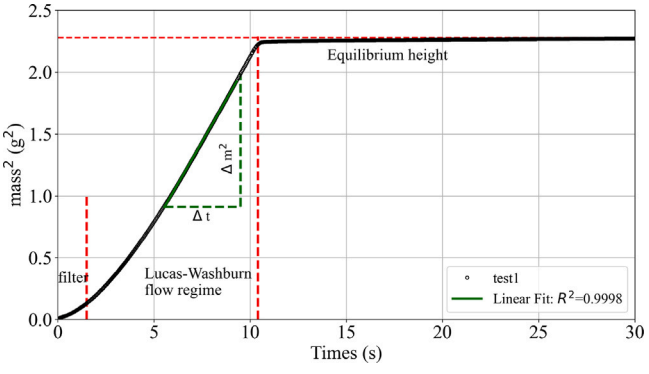

Fig. 4. Evolution of the flow front during a typical capillary rise through the cotton fiber with n-Heptane.

As shown in Fig. 5, a graph with dual y-axes is plotted to visualize the results. The left y-axis represents the R^2 values for all intervals, with a horizontal line marking the threshold (R^2=0.9998). The right y-axis

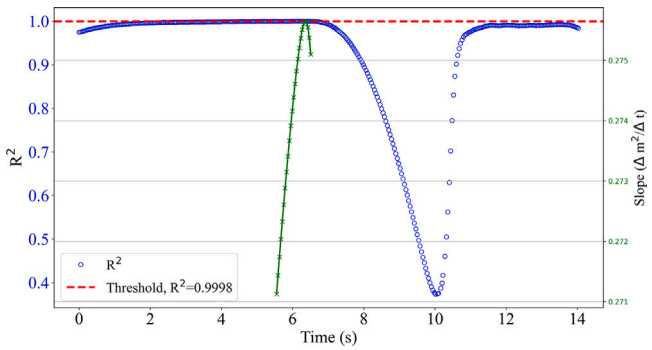

Fig. 5. Correlation coefficient and slope variation with time in Lucas–Washburn flow regime.

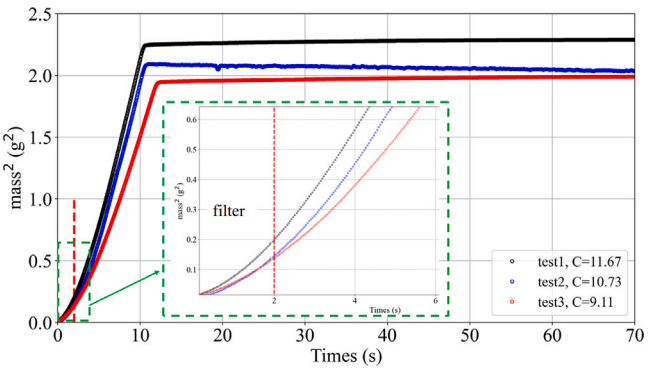

Fig. 6. Capillary rise test results with n-Heptane for cotton fiber samples.

Table 3
Geometric factor results from the tests.

	$\Delta m^2/\Delta t$ (g^2/s)	R^2	T (° C)	C (mm^5)	$c\tilde{r}$ (μ m)
Test1	0.273	0.99981	19.9	11.67	7.83
Test2	0.251	0.99980	20.78	10.73	7.20
Test3	0.213	0.99981	21.02	9.11	6.11
Average results				10.39 ± 1.28	6.97 ± 0.86

displays the slope ($\Delta m^2/\Delta t$) of the intervals that meet the $R^2 \geq 0.9998$) condition. Based on the results in Fig. 5, 24 intervals that meet the specified criteria (interval length of 4 s and $R^2 \geq 0.9998$) are identified, such as (5.55, 9.55), (5.59, 9.60), continuing until the final interval (6.51, 10.51). Within these intervals, the slope values ($\Delta m^2/\Delta t$) range from 0.271 to 0.276. These values are nearly constant, and an average slope of 0.273 is used as the final determined slope. This averaging approach minimizes the potential bias associated with selecting a single interval, ensuring a more robust and reliable estimation of the slope. For example, in the intervals where $R^2 \geq 0.9998$, the slope values range from 0.271 to 0.276. If a single slope value such as 0.271 were selected, the potential error could reach up to 1.85% ((0.276 - 0.271)/0.271). In contrast, by averaging the slope values, the final determined slope of 0.273 reduces the potential error to 1.10% ((0.276 - 0.273)/0.273), providing greater confidence in the reliability and accuracy of the results. While the improvement in this specific case may appear modest, it becomes more pronounced for fluids with higher viscosities, as demonstrated later in Fig. 10(c).

To determine the geometric factor (C) from the modified Washburn equation, three tests were conducted using n-heptane, a liquid that fully wets the solid substrate, applying the tensiometric method explained in Section 3.2.1. The geometric factor is determined based on the relationship between mass and the contact angle, which for n-heptane is zero. Specifically, the value of C or geometric product ($c\tilde{r}$) can be calculated using the following equation:

$$C = \frac{\Delta m^2}{\Delta t}\frac{\mu}{\rho^2\gamma_L}, \quad c\tilde{r} = \frac{2C}{\varepsilon^2(\pi R^2)^2} \tag{21}$$

The analysis follows the Lucas–Washburn assumptions, which neglect both inertial effects and gravitational forces. The slope of the intermediate Lucas–Washburn regime is sought across the different trials, as shown in Fig. 6. The calculated values of the geometric factor (C), along with the corresponding geometric product ($c\tilde{r}$) and the averaged results with errors, are presented in Table 3.

It was observed that in tests 1 through 3 (Table 3), the geometric factor values were reproducible [11.67, 10.73, 9.11] (in mm^5). The variation in the internal structure of each sample can account for the slight differences in the geometric factor observed across different tests. As mentioned in Section 3.2.2, even though the compression method described during sample preparation was used to homogenize the porosity, the geometry of the fibers remained inconsistent.

The curves obtained from the different tests exhibit the same shape as described by the Lucas–Washburn relationship. Ideally, for the same compression ratio, all curves should overlap, but this is not the case. The discrepancies arise due to variations in mass between each test, as the winding of the samples differed, leading to changes in volume and resulting in different compression ratios. To further validate the obtained geometric porous medium factor C or geometric product $c\tilde{r}$, a comparison was conducted with similar studies from the literature, as presented in Table 4. The geometric product was selected for comparison, as it eliminates the influence of varying capillary radius reported in the literature, providing a more accurate reflection of the natural fiber structures. The table summarizes the materials used, fluid types, and porosity values from these studies. Due to the compression applied to the cotton fibers in this work, finding identical studies for direct comparison was challenging. However, as shown in the table, for similar fiber structures such as flax fibers and porous paper, the $c\tilde{r}$ values generally fall around 7.0 ± 0.5, with specific values influenced by the porosity. The $c\tilde{r}$ value obtained in this study, 6.97 ± 0.86, aligns well with this range and reflects the structural characteristics of the compressed cotton fibers.

4.2. Determination of apparent advancing contact angles and surface free energy

In this subsection, the dynamic contact angles of two different liquids were determined using the corresponding geometric factor in Eq. (9): one highly viscous (glycerol) and the other less viscous (water). These measurements were conducted following the same protocol as previously described. The results of the various tests are presented below.

4.2.1. Water - cotton fibers

First, the case where the liquid is water is discussed. The apparent advancing contact angles of water on cotton fibers were measured using a KRÜSS instrument, with three independent tests conducted. The value of θ_a can be calculated using the following equation:

$$cos\theta_a = \frac{\Delta m^2}{\Delta t}\frac{\mu}{\rho^2\gamma_L C} \tag{22}$$

where C is 10.39 mm^5, as shown in Table 3. The results are shown in Fig. 7, illustrating that the relationship between the square of the absorbed mass (in g^2) and time (in seconds) follows a consistent pattern across all tests. Initially, a linear rise is observed (in the region to the left of the red dashed line) due to the presence of the paper filter. This is followed by a phase of rapid absorption, corresponding to the Lucas–Washburn flow regime, and then stabilization as the system reaches equilibrium.

The method for determining the linear fitting interval, described in Section 4.1, was employed. The same script was used to obtain the

Table 4
Comparison of geometric product with similar studies in the literature.

Year	Investigators	Materials	Fluids	Porosity	$c\tilde{r}$ (μ m)	Remarks
2018	Testoni et al. [8]	flax fiber	n-hexane	0.6	6.32 ± 0.09	substitute the data into Eqs. (9) and (21)
		flax fiber	n-hexane	0.65	7.03 ± 0.28	
		flax fiber	n-hexane	0.7	7.37 ± 0.39	
2023	Patari et al. [37]	porous paper	water	0.776	6.41 ± 0.13	substitute the data into Eqs. (9) and (21)
2024	This work	cotton fiber	n-heptane	0.483	6.97 ± 0.86	compressed the cotton fibers

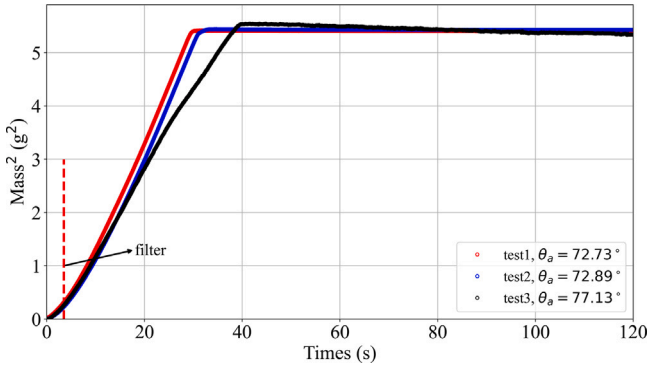

Fig. 7. Capillary rise test results with water for cotton fiber samples.

Table 5
Contact angle results from the tests for cotton fiber samples in water.

	$\Delta m^2/\Delta t$ (g^2/s)	R^2	T (° C)	θ_a (°)
Test1	0.220	0.99981	21.09	72.73
Test2	0.218	0.99980	21.09	72.89
Test3	0.165	0.99980	21.17	77.13
Average results				74.93 ± 2.20

results, and the correlation coefficient and slope variation over time for cotton fiber samples in water are displayed in Fig. 8. For test 1 (Fig. 8(a)), the selected fitting interval was (17.11, 27.11) with a length of 10 s, yielding an average slope of 0.220. For test 2 (Fig. 8(b)), the selected fitting interval was (18.11, 28.11), with a length of 10 s, and the calculated average slope was 0.218. For test 3 (Fig. 8), the chosen interval was (13.4, 23.4), also 10 s in length, with an average slope of 0.165. Specific data are presented in Table 5, where the measured apparent advancing contact angles were θ_a = 72.73°, θ_a = 72.89°, and θ_a = 77.13°, resulting in an average value of 74.93 ± 2.20, indicating a high level of reproducibility. The slight variations in mass absorption rates are attributed to differences in the cotton fiber structure or sample preparation. Overall, the results confirm the consistency and reliability of the capillary rise measurements within this system.

4.2.2. Glycerol - cotton fibers

Following the water tests, the apparent advancing contact angles of glycerol on cotton fibers were also measured using the KRÜSS instrument, with three independent tests conducted. The results, presented in Fig. 9, show the relationship between the square of the absorbed mass (in g^2) and time (in seconds). Due to glycerol's much higher dynamic viscosity – around 1500 times that of water – the absorption process took longer, and only the linear growth region is presented in Fig. 9.

Linear fitting intervals were determined, and the specific results are displayed in Fig. 10. For test 1, the chosen interval was (500, 750) seconds, with a length of 250 s and an average slope of 2.57×10^{-4}. For test 2, the selected interval was (750, 1000) seconds, with the same length, and the average slope calculated was 2.23×10^{-4}. For test 3, the fitting interval was also (750, 1000) seconds, with an average slope of 2.65×10^{-4}. The measured contact angles for glycerol were θ_a = 68.41°, θ_a = 71.38°, and θ_a = 67.71°, as shown in Table 6. It revealed slightly more variation between tests compared to water. This variation can be

Table 6
Contact angle results from the tests for cotton fiber samples in glycerol.

	$\Delta m^2/\Delta t$ (g^2/s)	R^2	T (° C)	θ_a (°)
Test1	2.57×10^{-4}	0.99981	21.27	68.41
Test2	2.23×10^{-4}	0.99980	20.56	71.38
Test3	2.65×10^{-4}	0.99981	20.42	67.71
Average results				69.55 ± 1.83

attributed to differences in fiber structure and the higher viscosity of glycerol, which affects the absorption rate.

Based on the results presented in Tables 5 and 6, it is clear that the apparent advancing contact angle is influenced by the surface tension between the liquid and the solid. The variability observed in different tests with the same liquid can be attributed to fluctuations in the surface tension of the samples, as the apparent advancing contact angle remains independent of the medium's porosity. The surface tensions of water and glycerol are 72.75 mN/m and 63.00 mN/m, respectively, with glycerol having a surface tension 15.5% ((72.75-63.00)/63.00) lower than that of water. Higher surface tension leads to a larger apparent advancing contact angle (for example, the average value in Table 5 is 74.93° ± 2.20°, while in Table 6 it is 69.55° ± 1.83°), as the contact angle reflects the adhesive forces between the liquid and the surface. This demonstrates that surface tension plays a critical role in minimizing the surface energy at the liquid–solid interface.

To further confirm the validity of the apparent advancing contact angles obtained in this study, a comparative analysis with data from similar research was performed, as detailed in Table 7.

This table compiles information on the materials studied, the fluids employed, and the associated porosity values from the literature. Since the cotton fibers in this work were compressed, finding studies with identical experimental conditions was difficult. However, for comparable fiber structures, such as flax fibers with a porosity of 0.6, θ_a values around 70.5±4.2 have been reported, demonstrating a clear dependence on porosity. The apparent advancing contact angles obtained in this work were measured as 74.93 ± 2.20 for water and 69.55 ± 1.83 for glycerol, indicating a reasonable agreement with previously reported trends for similar materials.

4.2.3. Surface free energy of cotton fiber

With all the advancing contact angles obtained, further analysis focused on the surface free energy (SFE), a thermodynamic quantity describing the equilibrium state of atoms in the surface layer of materials [39,40]. In this subsection, the Surface Free Energy (SFE) and its components were calculated using the well-established Owen-Wendt method [41] and the van Oss-Chaudhury-Good (vOCG) method [35].

The calculation of a solid's SFE (γ_S) from contact angle (θ) measurements is based on Young's equation [42], expressed as:

$$\gamma_L cos\theta = \gamma_S - \gamma_{SL} \tag{23}$$

where γ_{SL} is the interfacial free energy between the solid and liquid. A simple assumption was made, using the advancing contact angle (θ_a) values to represent the contact angle (θ) in Eq. (23). Suryadi et al. [34] outlined the following equations for calculating the SFE based on the Owen-Wendt (Eq. (24)) and vOCG (Eq. (25)) methods.

$$(1 + \cos\theta_a)\gamma_L = 2(\gamma_S^d \gamma_L^d)^{1/2} + 2(\gamma_S^p \gamma_L^p)^{1/2} \tag{24}$$

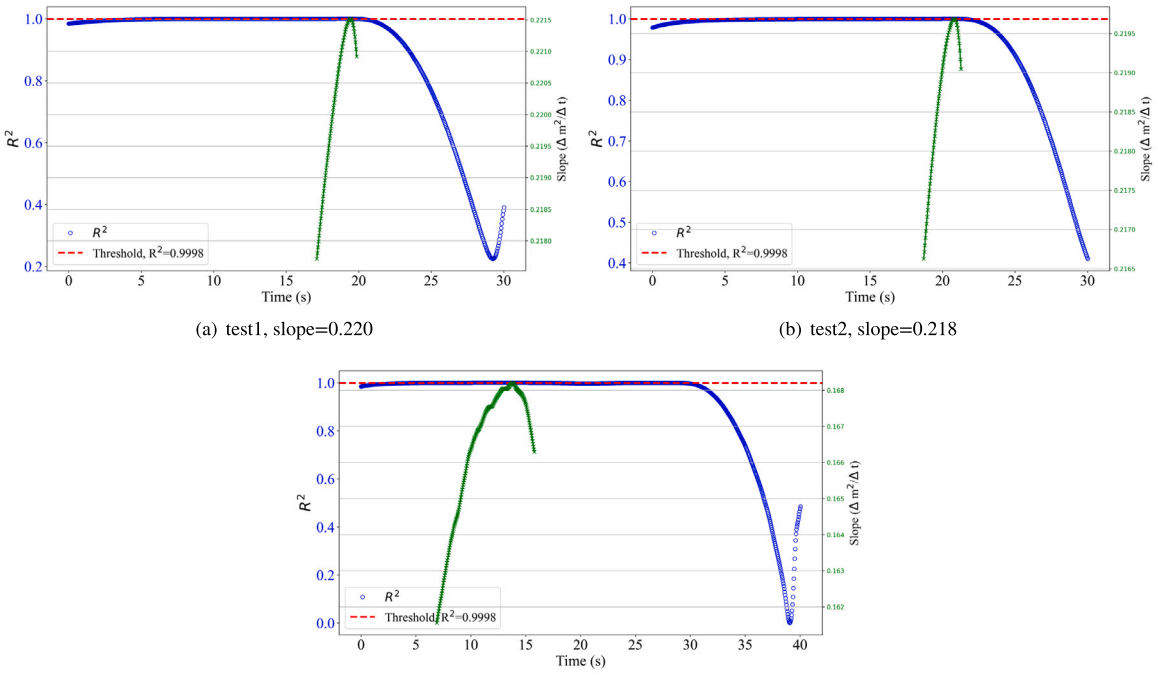

(a) test1, slope=0.220

(b) test2, slope=0.218

(c) test3, slope=0.165

Fig. 8. Correlation coefficient and slope variation over time for cotton fiber samples in water.

Table 7
Comparison of apparent advancing contact angles with similar studies in literature.

Year	Investigators	Materials	Fluids	Porosity	θ_a (°)	Remarks
2011	Fuentes et al. [38]	bamboo fibers	water	–	87.7 ± 14.7	non-autoclave treated fibers
		bamboo fibers	water	–	68.8 ± 3.2	autoclave treated fibers
2018	Testoni et al. [8]	flax fiber	water	0.6	70.5 ± 4.2	
		flax fiber	water	0.65	68.0 ± 4.8	
		flax fiber	water	0.7	62.4 ± 5.6	
2024	This work	cotton fiber	water	0.483	74.93 ± 2.20	compressed the cotton fibers
		cotton fiber	glycerol	0.483	69.55 ± 1.83	

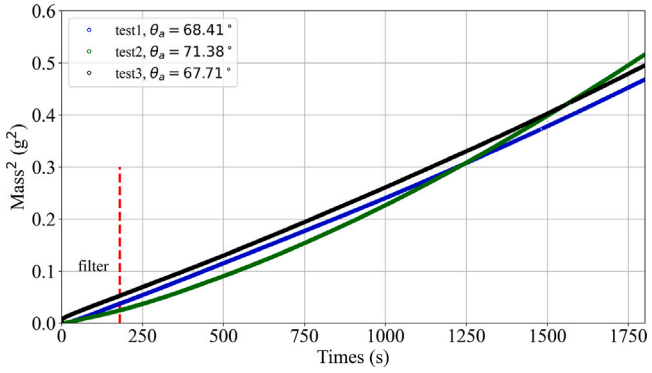

Fig. 9. Capillary rise test results with glycerol for cotton fiber samples.

$$(1+\cos\theta_a)\gamma_L = 2\left(\sqrt{\gamma_S^{LW}\gamma_L^{LW}} + \sqrt{\gamma_S^{+}\gamma_L^{-}} + \sqrt{\gamma_S^{-}\gamma_L^{+}}\right) \quad (25)$$

Detailed explanations are not provided here for the sake of conciseness. In Eq. (24), there are only two unknowns, γ_S^d, γ_S^p. By substituting the γ_L, γ_L^d and γ_L^p values for n-heptane and water from Table 2, along with the advancing contact angle data from Tables 5, these unknowns can be easily determined. In Eq. (25), there are three unknowns: γ_S^{LW}, γ_S^+, and γ_S^-. First, the γ_S^{LW} value is determined using the data for n-heptane, as both γ_L^+, γ_L^- and θ_a for n-heptane are zero. With γ_S^{LW} known, Eq. (25) reduces to two unknowns. By substituting the γ_L, γ_L^{LW} γ_L^+, and γ_L^- values for water and glycerol from Table 2, along with the advancing contact angle data for water and glycerol from Tables 5 and 6, all the unknowns can be solved. The detailed results are presented in Table 8.

The data presented in Table 8 shows that the total surface free energy (γ_S) of cotton fiber, calculated using the Owen-Wendt (OW) and van Oss-Chaudhury-Good (vOCG) methods, is 32.28 mN/m and 27.82 mN/m, respectively. The dispersive components (γ_S^d) obtained using the OW method are similar to those (γ_S^{LW}) calculated by the vOCG method and are higher than their corresponding polar components. In the vOCG method, the long-range interaction component (γ_S^{LW}) contributing 20.10 mN/m, more than the acid–base interaction component (γ_S^{AB}) at 7.72 mN/m. Furthermore, the Lewis base component (γ_S^-) is 15.68 mN/m, much higher than the Lewis acid component (γ_S^+) at 0.95 mN/m, indicating that cotton fiber surfaces predominantly exhibit electron-donating (basic) characteristics. To validate the accuracy of the obtained surface free energy values, a comparison was made with the work of Velde et al. [43], where the surface energy of flax fibers, subjected to different retting methods and treatments, was determined using a fiber floating approach with various test fluids. The reported values ranged between 29.7 and 34.2 mN/m, indicating that the value obtained in this study, 27.82 mN/m, falls within an acceptable range. Overall, the results highlight that the surface free energy of cotton fiber is primarily governed by non-polar long-range interactions, with relatively weak contributions from acid–base interactions.

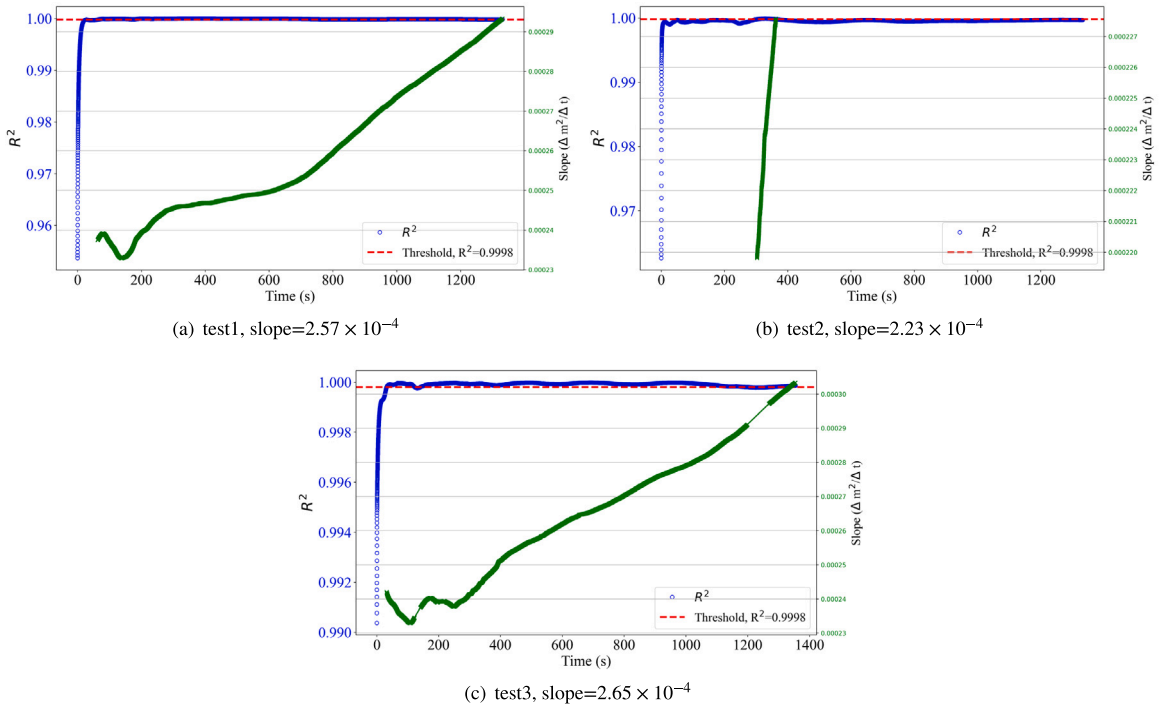

(a) test1, slope=2.57×10^{-4}

(b) test2, slope=2.23×10^{-4}

(c) test3, slope=2.65×10^{-4}

Fig. 10. Correlation coefficient and slope variation over time for cotton fiber samples in glycerol.

Table 8
Surface free energy and its components (mN/m) of cotton fiber calculated using the Owen-Wendt and vOCG methods.

Owen-Wendt method				
solid surface free energy γ_S ($\gamma_S^d+\gamma_S^p$)	dispersion part γ_S^d	polar part γ_S^p		
32.28	20.10	12.18		
vOCG method				
solid surface free energy γ_S ($\gamma_S^{LW}+\gamma_S^{AB}$)	long-range interactions γ_S^{LW}	acid–base interactions γ_S^{AB} ($2(\gamma_S^+\ \gamma_S^-)^{1/2}$)	acid component γ_S^+	base component γ_S^-
27.82	20.10	7.72	0.95	15.68

Table 9
Results of capillary pressure tests for various liquids in the sample with ε=0.483 and C=10.39 mm^5.

Liquids	n-heptane	Water	Glycerol
Capillary pressure (kPa)	2.65 ± 0.33	2.50 ± 0.31	2.91 ± 0.36

4.3. Determination of capillary pressure

Capillary pressure can be calculated using Eq. (17), where the geometric product $c\tilde{r}$, porosity ε, and apparent advancing contact angle θ_a are known, and permeability K is determined using Eq. (18). where the diameter of a single fiber r_f is within the range of 12–24 μm. However, given the compression applied, a value of 10 μm has been used [32]. Since the focus is on comparing the capillary pressure, note that the permeability of the sample remains unaffected by multiple measurements.

Using Eq. (18), the permeability is calculated to be 6.36×10^{-12} m^2. Substituting these values into Eq. (17) provides a set of values for the capillary pressure. The results for the three different liquids are presented in Table 9.

Firstly, the capillary pressure values obtained are consistent with the magnitude found in literature [17], all in the kPa range. Secondly, it can be observed that, compared to n-heptane and water, glycerol exhibits a higher capillary pressure. This difference is likely due to glycerol's higher viscosity, which increases the resistance to liquid movement through the fiber network, resulting in a higher pressure. Additionally, the slightly lower surface tension of glycerol compared to water may also contribute to this increase, as surface tension plays a critical role in capillary-driven flow. These observations suggest that the physicochemical properties of the liquid, such as viscosity and surface tension, influence the capillary pressure during impregnation.

5. Conclusion

The experimental method was used to determine the geometrical factors and the fluid/solid interaction (i.e., the apparent advancing contact angle), which were measured through capillary wicking in cotton fibers. Specifically, the geometrical factors, measured as 10.39 ± 1.28 mm^5, were determined via capillary rise tests with n-heptane for cotton fiber samples. During this process, a simple approach for selecting the linear fitting interval was introduced. Subsequently, two fluids with large different viscosities, water and glycerol, were used to perform tests on cotton fiber samples. The apparent advancing contact angle for water was found to be 74.93° ± 2.20°, while for glycerol it was 69.55°±1.83°. In comparison, water, which has a higher surface tension, exhibited a higher apparent advancing contact angle. Lastly, capillary pressure for the various liquids was calculated. For n-heptane, water, and glycerol, the capillary pressures were 2.65 ± 0.33, 2.50 ± 0.31, and 2.91 ± 0.36 kPa with ε=0.483 and C=10.39 mm^5, respectively. It was observed that glycerol, compared to n-heptane and water, exhibited a higher capillary pressure. This difference is likely due to glycerol's

higher viscosity, which increases resistance to liquid flow through the fiber network, resulting in elevated pressure. This study can be extended to different samples, encompassing a wider range of geometrical factors, and varying porosities (compression rates) to investigate their impact on capillary pressure.

CRediT authorship contribution statement

Shaolin Liu: Writing – review & editing, Writing – original draft, Methodology, Investigation. **Amine Ben-Abdelwahed:** Writing – review & editing, Validation, Supervision, Resources.

Declaration of competing interest

The authors declare that they have no known competing financial interests or personal relationships that could have appeared to influence the work reported in this paper.

Appendix. Numerical solution and analysis of the capillary rise equation

The numerical solution of the governing equation (Eq. (6)) was conducted without introducing additional terms, such as gravity or viscous resistance, to isolate the role of capillary forces in driving the liquid rise. The equation assumes a constant driving force, represented by $\frac{2\gamma_L cos\theta_a}{\rho r}$, which depends on the liquid surface tension (γ_L), the advancing contact angle (θ_a), the liquid density (ρ), and the capillary radius (r). The numerical solution was obtained using Python's *solve ivp* function with the Runge–Kutta method (RK45) [44], which is suitable for solving non-linear ordinary differential equations.

The simulation was performed with the following setup and steps:

1. The physical parameters used in the simulation were selected based on typical experimental values. γ_L was set to 72.75 mN/m, representing the surface tension of water, and θ_a was 74.93°, which was converted to radians for the computation. ρ was 1000 kg/m^3 representing the density of water, and r was 0.0005 m, reflecting a typical capillary size.
2. The governing equations (Eq. (6)), ($\left(\frac{dh}{dt}\right)^2 + h\left(\frac{d^2h}{dt^2}\right) = \frac{2\gamma_L cos\theta_a}{\rho r}$) was reformulated into a system of two first-order ordinary differential equations for numerical solution. By introducing $v = dh/dt$, the equation was split into:
$$\frac{dh}{dt} = v, \quad \frac{dv}{dt} = \frac{\frac{2\gamma_L cos\theta_a}{\rho r} - v^2}{h} \tag{26}$$
this transformation allows the use of numerical solvers to handle the non-linear system efficiently.
3. The initial conditions for the simulation were set as follows: the liquid column height at time $t = 0$ was initialized to $h(0) = 0.001$ m, and the initial velocity of the liquid column was set to $\frac{dh}{dt}(0) = 0$ m/s, assuming the liquid starts from rest.
4. The simulation was performed over a time range of $t = 0$ s to $t = 0.5$ s, with 500 evenly spaced evaluation points. This ensures sufficient resolution for accurately capturing the liquid column's dynamics.
5. To generalize the results and provide a dimensionless representation, the liquid height (h) was normalized by the theoretical maximum height (h_{max}), calculated as: $h_{max} = \frac{2\gamma_L cos\theta_a}{\rho g r}$, where g is the gravitational acceleration. Similarly, time (t) was normalized by the total simulation time (t_{max}=0.5s), resulting in dimensionless variables h/h_{max} and t/t_{max}.
6. The numerical computation was carried out using Python's *solve ivp* function [44]. The reformulated equations were integrated step-by-step, and the liquid column height and velocity were recorded at each time point.
7. Finally, the results were visualized in a dimensionless plot of normalized height (h/h_{max}) against normalized time (t/t_{max}), as shown in Fig. 11.

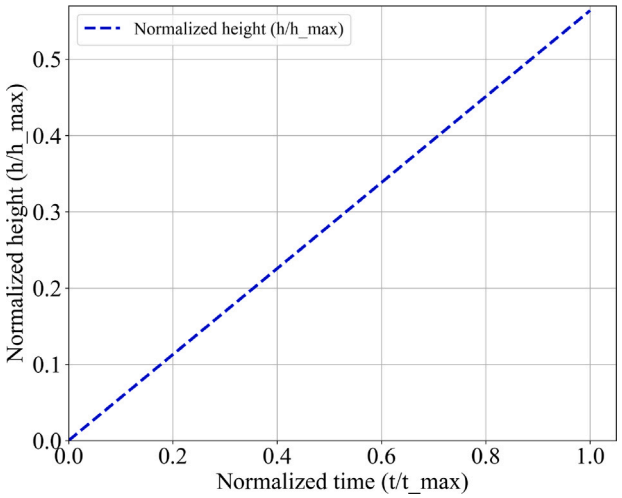

Fig. 11. Dimensionless height vs. time for capillary rise under constant driving force.

The normalized representation provides a general framework for interpreting the behavior of the system across different experimental conditions. It highlights the rapid initial acceleration of the liquid column due to capillary forces. The model effectively captures the early-stage dynamics of capillary rise but does not account for equilibrium effects, as it excludes gravitational and viscous terms, leading to a continuous growth of the liquid height over time.

Data availability

Data will be made available on request.

References

[1] J. Wang, G. Geng, X. Liu, F. Han, J. Xu, Magnetically superhydrophobic kapok fiber for selective sorption and continuous separation of oil from water, Chem. Eng. Res. Des. 115 (2016) 122–130, http://dx.doi.org/10.1016/j.cherd.2016.09.032.
[2] J. Wu, Z. Zhao, C. Jiang, Y. Yang, Z. Sun, J. Yuang, F. Xiao, Recent development and application of natural fiber in asphalt pavement, J. Clean. Prod. 449 (2024) 141832, http://dx.doi.org/10.1016/j.jclepro.2024.141832.
[3] K. Müller, E. Bugnicourt, M. Latorre, M. Jorda, Y. Echegoyen Sanz, J.M. Lagaron, O. Miesbauer, A. Bianchin, S. Hankin, U. Bölz, G. Pérez, M. Jesdinszki, M. Lindner, Z. Scheuerer, S. Castelló, M. Schmid, Review on the processing and properties of polymer nanocomposites and nanocoatings and their applications in the packaging, automotive and solar energy fields, Nanomaterials 7 (4) (2017) http://dx.doi.org/10.3390/nano7040074.
[4] B. Koohestani, A. Darban, P. Mokhtari, E. Yilmaz, E. Darezereshki, Comparison of different natural fiber treatments: a literature review, Int. J. Environ. Sci. Technol. 16 (2019) 629–642, http://dx.doi.org/10.1007/s13762-018-1890-9.
[5] K. Charlet, J.-P. Jernot, J. Breard, M. Gomina, Scattering of morphological and mechanical properties of flax fibres, Ind. Crop. Prod. 32 (3) (2010) 220–224, http://dx.doi.org/10.1016/j.indcrop.2010.04.015.
[6] J. Kim, H.-Y. Kim, On the dynamics of capillary imbibition, J. Mech. Sci. Technol. 26 (2012) 3795–3801, http://dx.doi.org/10.1007/s12206-012-1006-2.
[7] C. Wang, Z. Jin, D. Wang, Z. Li, H. Shen, M. Tian, Taylor bubble splitting, flow and coalescence in branching microchannels: An experimental and numerical simulation study, Chem. Eng. J. 486 (2024) 150231, http://dx.doi.org/10.1016/j.cej.2024.150231.
[8] G.A. Testoni, S. Kim, A. Pisupati, C.H. Park, Modeling of the capillary wicking of flax fibers by considering the effects of fiber swelling and liquid absorption, J. Colloid Interface Sci. 525 (2018) 166–176, http://dx.doi.org/10.1016/j.jcis.2018.04.064.
[9] H. Teixidó, J. Staal, B. Caglar, V. Michaud, Capillary effects in fiber reinforced polymer composite processing: a review, Front. Mater. 9 (2022) 809226, http://dx.doi.org/10.3389/fmats.2022.809226.

[10] L. Galet, S. Patry, J. Dodds, Determination of the wettability of powders by the washburn capillary rise method with bed preparation by a centrifugal packing technique, J. Colloid Interface Sci. 346 (2) (2010) 470–475, http://dx.doi.org/10.1016/j.jcis.2010.02.051.
[11] A. Mohammad Karim, W.J. Suszynski, Physics of dynamic contact line: Hydrodynamics theory versus molecular kinetic theory, Fluids 7 (10) (2022).
[12] D. Fu, C. Zhang, G. Wang, H. Na, Y. Wu, An update review of molecular dynamic study on thermal physical properties of molten salt, Sol. Energy Mater. Sol. Cells 273 (2024) 112916, http://dx.doi.org/10.1016/j.solmat.2024.112916.
[13] M.A.B. Abdelwahed, Y. Wielhorski, L. Bizet, J. Bréard, Bubble formation and transport in t-junction for application to liquid composite molding: Wetting effect, J. Compos. Mater. 48 (1) (2014) 37–48, http://dx.doi.org/10.1177/0021998312467553.
[14] Y. Wielhorski, M.A. Ben Abdelwahed, L. Bizet, J. Bréard, Wetting effect on bubble shapes formed in a cylindrical t-junction, Chem. Eng. Sci. 84 (2012) 100–106, http://dx.doi.org/10.1016/j.ces.2012.08.008.
[15] E.B. Dussan, On the spreading of liquids on solid surfaces: Static and dynamic contact lines, Annu. Rev. Fluid Mech. 11 (Volume 11 1979) (1979) 371–400, http://dx.doi.org/10.1146/annurev.fl.11.010179.002103.
[16] N. Fries, M. Dreyer, An analytic solution of capillary rise restrained by gravity, J. Colloid Interface Sci. 320 (1) (2008) 259–263, http://dx.doi.org/10.1016/j.jcis.2008.01.009.
[17] M.F. Pucci, P.-J. Liotier, S. Drapier, Capillary wicking in a fibrous reinforcement – orthotropic issues to determine the capillary pressure components, Composites A 77 (2015) 133–141, http://dx.doi.org/10.1016/j.compositesa.2015.05.031.
[18] S.F. Nia, K. Jessen, Theoretical analysis of capillary rise in porous media, Transp. Porous Media 110 (1) (2015) 141–155, http://dx.doi.org/10.1007/s11242-015-0562-1.
[19] H. Yao, A phase field method for convective phase change problem preserving maximum bound principle, Appl. Numer. Math. 204 (2024) 232–248, http://dx.doi.org/10.1016/j.apnum.2024.06.012.
[20] Q. Xiong, T.G. Baychev, A.P. Jivkov, Review of pore network modelling of porous media: Experimental characterisations, network constructions and applications to reactive transport, J. Contam. Hydrol. 192 (2016) 101–117, http://dx.doi.org/10.1016/j.jconhyd.2016.07.002.
[21] Y. Yang, R. Pan, Y. Wu, Q. Pan, Y. Shuai, A porous media catalyst for waste polyethylene pyrolysis in a continuous feeding reactor, Energy 302 (2024) 131855, http://dx.doi.org/10.1016/j.energy.2024.131855.
[22] R. Lucas, Ueber das zeitgesetz des kapillaren aufstiegs von flüssigkeiten, Kolloid-Zeitschrift 23 (1918) 15–22, https://api.semanticscholar.org/CorpusID:97596580.
[23] E.W. Washburn, The dynamics of capillary flow, Phys. Rev. 17 (1921) 273–283, http://dx.doi.org/10.1103/PhysRev.17.273.
[24] Y. Shiri, S.M.J. Seyed Sabour, Analytical, experimental, and numerical study of capillary rise dynamics from inertial to viscous flow, Phys. Fluids 34 (10) (2022) 102105, http://dx.doi.org/10.1063/5.0111688.
[25] M. Stange, M.E. Dreyer, H.J. Rath, Capillary driven flow in circular cylindrical tubes, Phys. Fluids 15 (9) (2003) 2587–2601, http://dx.doi.org/10.1063/1.1596913.
[26] B. Zhmud, F. Tiberg, K. Hallstensson, Dynamics of capillary rise, J. Colloid Interface Sci. 228 (2) (2000) 263–269, http://dx.doi.org/10.1006/jcis.2000.6951.
[27] D. Gründing, M. Smuda, T. Antritter, M. Fricke, D. Rettenmaier, F. Kummer, P. Stephan, H. Marschall, D. Bothe, A comparative study of transient capillary rise using direct numerical simulations, Appl. Math. Model. 86 (2020) 142–165, http://dx.doi.org/10.1016/j.apm.2020.04.020.
[28] N. Ichikawa, Y. Satoda, Interface dynamics of capillary flow in a tube under negligible gravity condition, J. Colloid Interface Sci. 162 (1994) 350–355, https://api.semanticscholar.org/CorpusID:93967028.
[29] A. Hamraoui, K. Thuresson, T. Nylander, V. Yaminsky, Can a dynamic contact angle be understood in terms of a friction coefficient? J. Colloid Interface Sci. 226 (2) (2000) 199–204, http://dx.doi.org/10.1006/jcis.2000.6830.
[30] D. Quéré, Inertial capillarity, Europhys. Lett. 39 (5) (1997) 533, http://dx.doi.org/10.1209/epl/i1997-00389-2.
[31] B. Gebart, Permeability of unidirectional reinforcements for rtm, J. Compos. Mater. 26 (8) (1992) 1100–1133, http://dx.doi.org/10.1177/002199839202600802.
[32] V. Rougier, Modélisation multi-échelle de l'imprégnation d'un milieu fibreux : morphologie, mouillage et perméabilité (Theses), Normandie Université, 2021.
[33] M.A. Ben Abdelwahed, Mécanismes d'imprégnation en milieux fibreux : Modélisation et application à la mise en oeuvre des matériaux composites à fibres longues Theses, Université du Havre, 2011, https://theses.hal.science/tel-00715952.
[34] G. Suryadi, S. Nikmatin, S. Sudaryanto, I. Sofian, S. Sukaryo, Surface free energy analysis of oil palm empty fruit bunches fiber reinforced biocomposites, IOP Conf. Ser. Earth Environ. Sci. 65 (2017) 012044, http://dx.doi.org/10.1088/1755-1315/65/1/012044.
[35] C.J. Van Oss, M.K. Chaudhury, R.J. Good, Interfacial lifshitz-van der waals and polar interactions in macroscopic systems, Chem. Rev. 88 (6) (1988) 927–941, http://dx.doi.org/10.1021/cr00088a006.
[36] S. Liu, A. Ahmadi-Senichault, C. Levet, J. Lachaud, Experimental investigation on the validity of the local thermal equilibrium assumption in ablative-material response models, Aerosp. Sci. Technol. 141 (2023) 108516, http://dx.doi.org/10.1016/j.ast.2023.108516.
[37] S. Patari, I.U. Chowdhury, J. Kumar, P.S. Mahapatra, Dynamics of liquid flow through fabric porous media: Experimental, analytical, and numerical investigation, Phys. Fluids 35 (10) (2023) 103305, http://dx.doi.org/10.1063/5.0166135.
[38] C. Fuentes, L. Tran, C. Dupont-Gillain, W. Vanderlinden, S. De Feyter, A. Van Vuure, I. Verpoest, Wetting behaviour and surface properties of technical bamboo fibres, Colloids Surf. A 380 (1) (2011) 89–99, http://dx.doi.org/10.1016/j.colsurfa.2011.02.032.
[39] B. Jańczuk, W. Wójcik, A. Zdziennicka, Determination of the components of the surface tension of some liquids from interfacial liquid-liquid tension measurements, J. Colloid Interface Sci. 157 (2) (1993) 384–393, http://dx.doi.org/10.1006/jcis.1993.1200.
[40] L. Ma, C. Zhang, Y. Wu, Y. Lu, Comparative review of different influence factors on molten salt corrosion characteristics for thermal energy storage, Sol. Energy Mater. Sol. Cells 235 (2022) 111485, http://dx.doi.org/10.1016/j.solmat.2021.111485.
[41] D.K. Owens, R.C. Wendt, Estimation of the surface free energy of polymers, J. Appl. Polym. Sci. 13 (8) (1969) 1741–1747, http://dx.doi.org/10.1002/app.1969.070130815.
[42] G. Cappelletti, S. Ardizzone, D. Meroni, G. Soliveri, M. Ceotto, C. Biaggi, M. Benaglia, L. Raimondi, Wettability of bare and fluorinated silanes: A combined approach based on surface free energy evaluations and dipole moment calculations, J. Colloid Interface Sci. 389 (1) (2013) 284–291, http://dx.doi.org/10.1016/j.jcis.2012.09.008.
[43] K. Van de Velde, P. Kiekens, Wettability of natural fibres used as reinforcement for composites, Die Angewandte Makromolekulare Chemie 272 (1) (1999) 87–93, http://dx.doi.org/10.1002/(SICI)1522-9505(19991201)272:1<87::AID-APMC87>3.0.CO;2-Q.
[44] J. Dormand, P. Prince, A family of embedded Runge-Kutta formulae, J. Comput. Appl. Math. 6 (1) (1980) 19–26, http://dx.doi.org/10.1016/0771-050X(80)90013-3.